

Charge symmetry breaking of the nucleon-nucleon interaction: ρ - ω mixing versus nucleon mass splitting

R. Machleidt^{1,*} and H. Mütter^{2,†}

¹*Department of Physics, University of Idaho, Moscow, Idaho 83844, U. S. A.*

²*Institut für Theoretische Physik, Universität Tübingen, D-72076 Tübingen, Germany*

(October 25, 2018)

Abstract

We investigate three models for the charge symmetry breaking (CSB) of the nucleon-nucleon (NN) interaction (based upon ρ - ω mixing, nucleon mass splitting, and phenomenology) that all reproduce the empirical value for the CSB of the 1S_0 scattering length (Δa_{CSB}) accurately. We reveal that these models make very different predictions for CSB in 3P_J waves and examine the impact of this on some observable quantities of $A \geq 3$ nuclear systems. It turns out that the ^3H - ^3He binding energy difference is essentially ruled by Δa_{CSB} and not very sensitive to CSB from P waves. However, the Coulomb displacement energies (which are the subject of the Nolen-Schiffer anomaly) receive about 50% of their CSB contribution from NN partial waves beyond 1S_0 . Consequently, the predictions by the various CSB models differ here substantially (10-20%). Unfortunately, the evaluation of the leading Coulomb contributions carry a large uncertainty such that no discrimination between the competing CSB models can presently be made. To decide the issue we suggest to look into nuclear few-body reactions that are sensitive to CSB of the nuclear force.

PACS numbers: 24.80.+y, 11.30.Hv, 13.75.Cs, 21.10.Sf, 21.45.+v

Typeset using REVTeX

*e-mail address: machleid@uidaho.edu

†e-mail address: herbert.muether@uni-tuebingen.de

I. INTRODUCTION

By definition, *charge independence* is invariance under any rotation in isospin space. A violation of this symmetry is referred to as charge dependence or charge independence breaking (CIB). *Charge symmetry* is invariance under a rotation by 180° about the y -axis in isospin space if the positive z -direction is associated with the positive charge. The violation of this symmetry is known as charge symmetry breaking (CSB). Obviously, CSB is a special case of charge dependence.

CIB of the strong NN interaction means that, in the isospin $T = 1$ state, the proton-proton ($T_z = +1$), neutron-proton ($T_z = 0$), or neutron-neutron ($T_z = -1$) interactions are (slightly) different, after electromagnetic effects have been removed. CSB of the NN interaction refers to a difference between proton-proton (pp) and neutron-neutron (nn) interactions, only.

Charge asymmetry is seen most clearly in the 1S_0 scattering length. The latest empirical values of the neutron-neutron (nn) singlet effective range parameters (corrected for electromagnetic effects) are

$$a_{nn}^N = -18.9 \pm 0.4 \text{ fm} [1, 2], \quad r_{nn}^N = 2.75 \pm 0.11 \text{ fm} [3]. \quad (1.1)$$

This should be compared to the corresponding proton-proton (pp) values [3]:

$$a_{pp}^N = -17.3 \pm 0.4 \text{ fm}, \quad r_{pp}^N = 2.85 \pm 0.04 \text{ fm}. \quad (1.2)$$

The implication is that the singlet effective range parameters break charge-symmetry by the following amounts,

$$\Delta a_{CSB} \equiv a_{pp}^N - a_{nn}^N = 1.6 \pm 0.6 \text{ fm}, \quad (1.3)$$

$$\Delta r_{CSB} \equiv r_{pp}^N - r_{nn}^N = 0.10 \pm 0.12 \text{ fm}. \quad (1.4)$$

The current understanding is that—on a fundamental level—the charge dependence of nuclear forces is due to a difference between the up and down quark masses and electromagnetic interactions among the quarks. As a consequence of this—on the hadronic level—major causes of CIB are mass differences between hadrons of the same isospin multiplet, meson mixing, and irreducible meson-photon exchanges. For recent reviews on charge dependence, see Refs. [3–5].

Neutral mesons with the same spin and parity, but different isospin, may mix due to the up-down quark mass difference and electromagnetic interactions; that is, the Hamiltonian responsible for the mixing, H_m , has a strong and an electromagnetic part,

$$H_m = H_{str} + H_{em}. \quad (1.5)$$

The most prominent case is ρ^0 - ω mixing that is observed in the annihilation process $e^+e^- \rightarrow \pi^+\pi^-$ from which the mixing matrix element has been extracted [6] to be

$$\langle \rho^0 | H_m | \omega \rangle = -0.00452 \pm 0.0006 \text{ GeV}^2. \quad (1.6)$$

The charge-asymmetric nuclear force created by this process is displayed in Fig. 1. Coon and Barrett showed [6] that this mechanism alone can explain the entire empirical CSB of

the singlet scattering length, Eq. (1.3). Other examples of meson mixing are π - η and π - η' mixing which, however, generate only negligible effects [7].

In recent years, the process of Fig. 1 has been subjected to some criticism. Note that the matrix element, Eq. (1.6), is extracted on-shell, i. e., for $k^2 = m_\rho^2$, where k denotes the four-momentum of the ρ meson and m_ρ the ρ mass. However, in the NN interaction, Fig. 1, the relevant k^2 are space-like (less than zero). Using a quark model for H_{str} , Goldman, Henderson, and Thomas [8] find a substantial k^2 dependence which is such that the contributions of Fig. 1 would nearly vanish. Similar results were reported in subsequent papers [9–11]. On the other hand, Miller [5] and Coon and coworkers [12] have advanced counter-arguments that would restore the traditional role of ρ - ω exchange. The issue is unresolved. Informative summaries of the controversial points of view can be found in Refs. [5,13,14].

We now turn to another basic source for CSB of the nuclear force, namely, nucleon mass splitting. The most trivial consequence of nucleon mass splitting is a difference in the kinetic energies: for the heavier neutrons, the kinetic energy is smaller than for protons. This raises the magnitude of the nn scattering length by 0.25 fm as compared to pp . Besides this, nucleon mass splitting has an impact on all meson-exchange diagrams that contribute to the nuclear force. For example, there are the one-boson exchange (OBE) diagrams, Fig. 2, which are affected by only a negligible amount. However, a sophisticated and realistic meson model for the nuclear force [15] goes beyond single meson exchange and includes irreducible diagrams of two-boson exchange which generate substantial CSB from nucleon mass splitting. The major part of the CSB effect comes from diagrams of 2π exchange with $N\Delta$ intermediate states, Fig. 3. In fact, these diagrams can fully explain the empirical CSB splitting of the singlet scattering length [16,17].

Finally, for reasons of completeness, we mention that irreducible diagrams of π and γ exchange between two nucleons create a charge-dependent nuclear force. Recently, these contributions have been calculated to leading order in chiral perturbation theory [18]. It turns out that to this order the $\pi\gamma$ force is charge-symmetric (but does break charge independence).

The bottom line then is that we have two CSB mechanisms in hand, each powerful enough to fully explain the charge asymmetry seen in the singlet scattering length. This state of affairs challenges the question: *Which of the two mechanisms is nature really using?* To answer the question, the 1S_0 state at zero energy is obviously of no use since this can be described equally well by both mechanisms. Thus, the answer, if any, can only come from energies $T_{lab} > 0$ and/or states with $L > 0$. It is quite possible that the predictions by the two mechanisms are very different in states other than 1S_0 . The 2π exchange contribution to the nuclear force (where the CSB effect due to nucleon mass splitting mainly comes from) is chiefly a central force of intermediate range, while vector meson exchange (involved in ρ - ω mixing) creates a large spin-orbit component and a short-ranged central force. This may create large differences in triplet P waves where the signature of spin-orbit forces is most pronounced. If large differences between the models occur for $L > 0$, then each mechanism may have a characteristic signature on observables that are sensitive to CSB from P and higher partial waves. In Ref. [19] it was found that about 50% of the CSB contribution to the Nolen-Schiffer (NS) anomaly [20] comes from the $L > 0$ two-nucleon states. Thus, there is the possibility that the differences between competing CSB models may show up as differences in the predictions for the NS anomaly. Other observables may be considered,

too.

It is the purpose of this paper to look into this issue. In particular, we want to find out if it is possible to discriminate between the two models for CSB based upon their predictions for observable quantities, other than the singlet scattering length.

Besides the two CSB mechanisms discussed, we will include in our study also a phenomenological model for CSB, namely, the Argonne V_{18} potential [21]. The three models will be introduced in Sec. II and applied to the ${}^3\text{H}$ - ${}^3\text{He}$ binding energy difference and the NS anomaly in Sec. III. Sec. IV concludes the paper.

II. MODELS FOR CHARGE SYMMETRY BREAKING OF THE TWO-NUCLEON INTERACTION

A. ρ - ω mixing

Here we will evaluate the charge asymmetric nuclear force generated by ρ^0 - ω mixing shown in Fig. 1 [22].

The coupling of ρ and ω mesons to nucleons is described by the following Lagrangians:

$$\mathcal{L}_{\omega NN} = -g_\omega \bar{\psi} \gamma^\mu \psi \varphi_\mu^{(\omega)}, \quad (2.1)$$

$$\mathcal{L}_{\rho NN} = -g_\rho \bar{\psi} \gamma^\mu \boldsymbol{\tau} \psi \cdot \boldsymbol{\varphi}_\mu^{(\rho)} - \frac{f_\rho}{4M_p} \bar{\psi} \sigma^{\mu\nu} \boldsymbol{\tau} \psi \cdot (\partial_\mu \boldsymbol{\varphi}_\nu^{(\rho)} - \partial_\nu \boldsymbol{\varphi}_\mu^{(\rho)}), \quad (2.2)$$

where ψ denotes nucleon fields, φ meson fields, and τ_i ($i = 1, 2, 3$) are the usual Pauli matrices describing isospin $\frac{1}{2}$; specifically, $\tau_3|p\rangle = +|p\rangle$ and $\tau_3|n\rangle = -|n\rangle$ with $|p\rangle$ a proton state and $|n\rangle$ a neutron state. M_p is the proton mass which is used as scaling mass in the ρNN Lagrangian to make f_ρ dimensionless. To avoid the creation of unmotivated charge dependence, the scaling mass M_p is used in pp as well as nn scattering.

The first Feynman diagram of Fig. 1 leads to the following ρ - ω potential,

$$\begin{aligned} \langle \mathbf{q}' \lambda'_1 \lambda'_2 | V_{\rho\omega}^{(1)} | \mathbf{q} \lambda_1 \lambda_2 \rangle &= -\frac{1}{(2\pi)^3} \sqrt{\frac{M}{E'}} \sqrt{\frac{M}{E}} \langle \rho^0 | H_m | \omega \rangle g_\rho g_\omega \\ &\times \bar{u}(\mathbf{q}', \lambda'_1) \tau_3 \left[\gamma_\mu + \frac{\kappa_\rho}{2M_p} \sigma_{\mu\nu} i(q' - q)^\nu \right] u(\mathbf{q}, \lambda_1) \\ &\times \bar{u}(-\mathbf{q}', \lambda'_2) \gamma^\mu u(-\mathbf{q}, \lambda_2) \\ &\times \frac{\mathcal{F}_\rho[(\mathbf{q}' - \mathbf{q})^2] \mathcal{F}_\omega[(\mathbf{q}' - \mathbf{q})^2]}{[(\mathbf{q}' - \mathbf{q})^2 + m_\rho^2][(\mathbf{q}' - \mathbf{q})^2 + m_\omega^2]}, \end{aligned} \quad (2.3)$$

where M denotes the relevant nucleon mass (i. e., $M = M_p$ in pp scattering and $M = M_n$ in nn scattering), m_α are meson masses, and $\kappa_\rho \equiv f_\rho/g_\rho$. We are working here in the two-nucleon c.m. frame and use the helicity formalism. The helicity λ_i of nucleon i is defined as the eigenvalue of the helicity operator $\frac{1}{2}\boldsymbol{\sigma}_i \cdot \mathbf{p}_i/|\mathbf{p}_i|$ which is $\pm\frac{1}{2}$. In-coming nucleon 1 carries helicity λ_1 and momentum \mathbf{q} and in-coming nucleon 2 carries helicity λ_2 and momentum $-\mathbf{q}$; the out-going nucleons have λ'_1 , \mathbf{q}' and λ'_2 , $-\mathbf{q}'$. The above ‘quasi-potential’ is defined in the framework of the relativistic, three-dimensional Blankenbecler-Sugar (BbS) equation [23] which is a reduced version of the four-dimensional relativistic Bethe-Salpeter

equation [24]. In the BbS formalism, the four-momentum transfer between the two nucleons is $(q' - q)^\mu = (0, \mathbf{q}' - \mathbf{q})$. The square-root factor $M/\sqrt{E'E}$ (with $E \equiv \sqrt{M^2 + \mathbf{q}^2}$ and $E' \equiv \sqrt{M^2 + \mathbf{q}'^2}$) makes it possible to cast the BbS equation into a form that is identical to the conventional Lippmann-Schwinger equation. The Dirac spinors in helicity representation are given by

$$u(\mathbf{q}, \lambda_1) = \sqrt{\frac{E+M}{2M}} \begin{pmatrix} 1 \\ \frac{2\lambda_1|\mathbf{q}|}{E+M} \end{pmatrix} |\lambda_1\rangle, \quad (2.4)$$

$$u(-\mathbf{q}, \lambda_2) = \sqrt{\frac{E+M}{2M}} \begin{pmatrix} 1 \\ \frac{2\lambda_2|\mathbf{q}|}{E+M} \end{pmatrix} |\lambda_2\rangle, \quad (2.5)$$

with normalization

$$\bar{u}(\mathbf{q}, \lambda)u(\mathbf{q}, \lambda) = 1, \quad (2.6)$$

where $\bar{u} \equiv u^\dagger \gamma^0$. The above amplitude, includes form factors

$$\mathcal{F}_\alpha[(\mathbf{q}' - \mathbf{q})^2] = \frac{\Lambda_\alpha^2 - m_\alpha^2}{\Lambda_\alpha^2 + (\mathbf{q}' - \mathbf{q})^2} \quad (2.7)$$

with m_α the mass of the meson involved and Λ_α the so-called cutoff mass. For more details concerning the formalism and the explicit evaluation of quasi-potentials of this kind, see Appendix E of Ref. [15].

The second Feynman diagram of Fig. 1 yields the same as the first one and, so, the entire ρ - ω potentials is

$$V_{\rho\omega} = 2V_{\rho\omega}^{(1)} \quad (2.8)$$

with $V_{\rho\omega}^{(1)}$ given by Eq. (2.3). Since $\langle \rho^0 | H_m | \omega \rangle$ is negative, $V_{\rho\omega}$ is repulsive for pp scattering and attractive for nn scattering with the magnitude of $V_{\rho\omega}$ essentially the same in both cases.

When constructing CSB NN potentials, one starts with the pp potential since there are many pp data (and pp phase shift analyses) of high quality to constrain the pp potential. In this work, we use the CD-Bonn pp potential [25] which reproduces the world pp data below 350 MeV lab. energy available in the year of 2000 with the perfect χ^2/datum of 1.01. The nn potential is then fabricated by adding to the pp potential a difference-potential that contains the entire difference between nn and pp due to ρ - ω exchange, which is

$$\Delta V_{\rho\omega} = V_{\rho\omega}(nn) - V_{\rho\omega}(pp) \approx -4\check{V}_{\rho\omega}^{(1)}(M_n) \quad (2.9)$$

where $\check{V}_{\rho\omega}^{(1)}$ is $V_{\rho\omega}^{(1)}$ [Eq. (2.3)] with the τ_3 operator replaced by 1. Note that—strictly speaking— $V_{\rho\omega}(nn)$ is to be evaluated with $M = M_n$ and $V_{\rho\omega}(pp)$ with $M = M_p$. However, if we wish to subsume both terms into one, then we have to use the same mass for both for which we choose $M = M_n$. We have tested this approximation and found that it affects the singlet scattering length by 10^{-4} fm.

To obtain a convenient expression for $\Delta V_{\rho\omega}$, we make use of the identity

$$\frac{1}{[(\mathbf{q}' - \mathbf{q})^2 + m_\rho^2][(\mathbf{q}' - \mathbf{q})^2 + m_\omega^2]} = \frac{1}{m_\omega^2 - m_\rho^2} \left[\frac{1}{(\mathbf{q}' - \mathbf{q})^2 + m_\rho^2} - \frac{1}{(\mathbf{q}' - \mathbf{q})^2 + m_\omega^2} \right], \quad (2.10)$$

which allows us to write $\Delta V_{\rho\omega}$ in terms of the difference of two expressions each of which resembles single meson exchange; namely,

$$\Delta V_{\rho\omega} = \Delta V_{\rho\omega}^{(\rho)} - \Delta V_{\rho\omega}^{(\omega)} \quad (2.11)$$

with

$$\begin{aligned} \langle \mathbf{q}' \lambda'_1 \lambda'_2 | \Delta V_{\rho\omega}^{(\rho)} | \mathbf{q} \lambda_1 \lambda_2 \rangle &= \frac{4}{(2\pi)^3} \sqrt{\frac{M}{E'}} \sqrt{\frac{M}{E}} \frac{\langle \rho^0 | H_m | \omega \rangle}{m_\omega^2 - m_\rho^2} g_\rho g_\omega \\ &\times \bar{u}(\mathbf{q}', \lambda'_1) \left[\gamma_\mu + \frac{\kappa_\rho}{2M_p} \sigma_{\mu\nu} i(q' - q)^\nu \right] u(\mathbf{q}, \lambda_1) \\ &\times \bar{u}(-\mathbf{q}', \lambda'_2) \gamma^\mu u(-\mathbf{q}, \lambda_2) \\ &\times \frac{\mathcal{F}_\rho[(\mathbf{q}' - \mathbf{q})^2] \mathcal{F}_\omega[(\mathbf{q}' - \mathbf{q})^2]}{(\mathbf{q}' - \mathbf{q})^2 + m_\rho^2}, \end{aligned} \quad (2.12)$$

and

$$\begin{aligned} \langle \mathbf{q}' \lambda'_1 \lambda'_2 | \Delta V_{\rho\omega}^{(\omega)} | \mathbf{q} \lambda_1 \lambda_2 \rangle &= \frac{4}{(2\pi)^3} \sqrt{\frac{M}{E'}} \sqrt{\frac{M}{E}} \frac{\langle \rho^0 | H_m | \omega \rangle}{m_\omega^2 - m_\rho^2} g_\rho g_\omega \\ &\times \bar{u}(\mathbf{q}', \lambda'_1) \left[\gamma_\mu + \frac{\kappa_\rho}{2M_p} \sigma_{\mu\nu} i(q' - q)^\nu \right] u(\mathbf{q}, \lambda_1) \\ &\times \bar{u}(-\mathbf{q}', \lambda'_2) \gamma^\mu u(-\mathbf{q}, \lambda_2) \\ &\times \frac{\mathcal{F}_\rho[(\mathbf{q}' - \mathbf{q})^2] \mathcal{F}_\omega[(\mathbf{q}' - \mathbf{q})^2]}{(\mathbf{q}' - \mathbf{q})^2 + m_\omega^2}. \end{aligned} \quad (2.13)$$

For the masses involved, we use [26],

$$M_p = 938.27231 \text{ MeV}, \quad (2.14)$$

$$M = M_n = 939.56563 \text{ MeV}, \quad (2.15)$$

$$m_\rho = 769.9 \text{ MeV}, \quad (2.16)$$

$$m_\omega = 781.94 \text{ MeV}, \quad (2.17)$$

and $\Lambda_\rho = \Lambda_\omega = 1.4 \text{ GeV}$.

We choose for the meson-nucleon coupling constants,

$$\frac{g_\rho^2}{4\pi} = 0.84, \quad (2.18)$$

$$\kappa_\rho = 6.1, \quad (2.19)$$

$$\frac{g_\omega^2}{4\pi} = 10, \quad (2.20)$$

and for the mixing matrix element,

$$\langle \rho^0 | H_m | \omega \rangle = -0.00402 \text{ GeV}^2, \quad (2.21)$$

to obtain

$$\Delta a_{CSB} = 1.508 \text{ fm}. \quad (2.22)$$

The above mixing matrix element is consistent with the empirical value, Eq. (1.6), and the ρ parameters are identical to the ones used in the Bonn Full Model [15]. Concerning the ω , the Bonn model uses $g_\omega^2/4\pi = 20$ which, however, would generate too much CSB when applied in the above ρ - ω potential; therefore our choice Eq. (2.20). This choice could be justified with the argument that part of the ω contribution in meson-theoretic potentials may be just a parametrization of short-ranged repulsion that is actually due to quark-gluon exchange.

To check our calculations, we have made a comparison with the results by Coon and Barrett [6]. Note that these authors use very different vector-meson coupling constants as compared to ours. In terms of our convention for the coupling constants, Eqs. (2.1) and (2.2) [27], Coon and Barrett use $g_\rho^2/4\pi = 0.6$, $\kappa_\rho = 3.7$, $g_\omega^2/4\pi = 5.25$, and $\kappa_\omega = -0.12$. There are also other differences, like, we use the the full relativistic Feynman amplitudes for ρ^0 - ω exchange, Eq. (2.3), while in Ref. [6] the nonrelativistic approximation is applied. Moreover, Coon and Barrett use the Reid potential [28] as their basic pp potential whereas we use the pp CD-Bonn [25]. Taking all these differences into account, we were able to show that our results are consistent with the findings of Coon and Barrett.

The bottom line is that due the uncertainties in the model parameters, there is latitude of a factor of two or so in the strength of the ρ - ω potential. Within that latitude, it is easy to fit the full amount of CSB of the singlet scattering length.

B. Nucleon mass splitting

The difference between the masses of neutron and proton represents a basic cause for CSB of the nuclear force. This source of CSB effects has been explored in great detail in [17]. The investigation is based upon the Bonn model for the NN interaction [15]. Let us briefly summarize the results. For this we divide the total number of meson exchange diagrams that is involved in the nuclear force into several classes. Below, we report the results for each class separately.

1. **One-boson-exchange** (OBE, Fig. 2) contributions mediated by $\pi^0(135)$, $\rho^0(770)$, $\omega(782)$, $a_0/\delta(980)$, and $\sigma'(550)$. In the Bonn model [15], the σ' describes only the correlated 2π exchange in $\pi\pi - S$ -wave (and not the uncorrelated 2π exchange since the latter is calculated explicitly, cf. Fig. 3). Charge-symmetry is broken by the fact that for pp scattering the proton mass is used in the Dirac spinors representing the four external legs [Fig. 2(a)], while for nn scattering the neutron mass is applied [Fig. 2(b)]. The CSB effect from the OBE diagrams is very small.
2. **2π -exchange diagrams.** This class consists of three groups; namely the diagrams with NN , $N\Delta$ and $\Delta\Delta$ intermediate states, where Δ refers to the baryon with spin and isospin $\frac{3}{2}$ and mass 1232 MeV. The most important group is the one with $N\Delta$

intermediate states which we show in Fig. 3. Part (a) of Fig. 2 applies to pp scattering, while part (b) refers to nn scattering. When charged-pion exchange is involved, the intermediate-state nucleon differs from that of the external legs. This is one of the sources for CSB from this group of diagrams. The 2π class of diagrams causes the largest CSB effect.

3. **$\pi\rho$ -exchanges.** Graphically, the $\pi\rho$ diagrams can be obtained by replacing in each 2π diagram (e. g., in Fig. 3) one pion by a ρ -meson of the same charge state. The effect is typically opposite to the one from 2π exchange.
4. **Further 3π and 4π contributions** ($\pi\sigma + \pi\omega$). The Bonn potential also includes some 3π -exchanges that can be approximated in terms of $\pi\sigma$ diagrams and 4π -exchanges of $\pi\omega$ type. The sum of the two groups is small, indicating convergence of the diagrammatic expansion. The CSB effect from this class is essentially negligible.

The total CSB difference of the singlet scattering length caused by nucleon mass splitting amounts to 1.508 fm [29] which agrees well with the empirical value 1.6 ± 0.6 fm. Thus, nucleon mass splitting alone can explain the entire empirical CSB of the singlet scattering length.

Starting from the CD-Bonn pp potential [25], the parameters of the scalar-isoscalar bosons of that model have been adjusted such that the microscopically evaluated phase shift differences due to nucleon mass splitting are reproduced accurately. This yields the CD-Bonn nn potential.

C. Phenomenological model

An excellent example for a phenomenological construction of the CSB nuclear force is the recent Argonne V_{18} NN potential [21]. As usual, the Argonne pp potential is fixed by a best-fit to the pp data. The Argonne nn potential is then constructed by starting from the pp one and readjusting the central force in the $S = 0, T = 1$ state such that the empirical value for a_{nn} is reproduced. For the $S = 1, T = 1$ state, where empirical information on nn scattering is not available, it is assumed that the CSB splitting of the central force is the same as in $S = 0, T = 1$.

D. Comparing the predictions for the two-nucleon system

In Table I, we show the 1S_0 effective range parameters as calculated by the three models applied in this study. By construction, the ρ - ω potential produces the same CSB difference as the nucleon mass (M_N) splitting model, namely, $\Delta a_{CSB} = 1.508$ fm. The Argonne V_{18} potential yields $\Delta a_{CSB} = 1.654$ fm. Thus, all three models have nearly identical results for Δa_{CSB} which is exactly what we want as the starting point of our study.

We now turn to energies $T_{lab} > 0$ and calculate the CSB phase shift differences $\Delta\delta_{CSB} \equiv \delta_{nn} - \delta_{pp}$ (without electromagnetic interactions) for all three models (see Fig. 4). In the 1S_0 state at low energies, we have, of course, nearly identical phase shift differences because of the agreement in Δa_{CSB} . However, as the energy increases, differences between the model

predictions emerge. The ρ - ω model maintains the largest $\Delta\delta_{CSB}$ above 150 MeV which may be explained by the fact that ρ - ω exchange is of shorter range than the 2π exchange which the M_N splitting CSB potential is based upon. The differences in 1D_2 can be explained with the same argument.

The largest differences between the model predictions occur in the 3P_J waves (cf. Fig. 4). As expected, the ρ - ω potential now clearly reveals its large spin-orbit component typical for vector-meson exchange. Note that the spin-orbit force of $\Delta V_{\rho\omega}$ is of opposite sign as the one of ordinary one-omega exchange [cf. Eqs. (2.9) and (2.3) and keep in mind that $\langle\rho^0|H_m|\omega\rangle$ is negative].

The Argonne V_{18} potential follows in 1S_0 the trend of the ρ - ω mechanism and in 3P_0 it is close to the M_N -splitting model. In the other partial waves, it is not close to any of the microscopic models for CSB.

In summary, in spite of identical Δa_{CSB} , the ρ - ω and the M_N -splitting models show drastic differences in 3P_J waves. Unfortunately, we do not have any empirical information on $\Delta\delta_{CSB}$ and, so, there is no direct way to tell which is right and which is wrong. Apart from the 1S_0 scattering lengths, the only empirical information on CSB that we have are some binding energy differences, to which P waves do contribute. Therefore, we will turn in the next section to such binding energy differences with the hope that the differences in P waves may impress a detectable signature.

III. PREDICTIONS FOR SYSTEMS WITH $A > 2$

A. ^3H - ^3He binding energy difference

The experimental value for the difference between the binding energies of ^3H and ^3He is 764 keV (^3H is more bound). Most of this difference is due to the static Coulomb energy (amongst finite-size protons) which accounts for 648 ± 4 keV [32–34]. Another 35 ± 3 keV come from electromagnetic effects neglected in the static Coulomb approximation [34,35] and 14 ± 2 keV are due to the $n - p$ mass difference in the kinetic energy [36]. After all these obvious corrections, a binding energy difference of 67 ± 9 keV remains which is commonly attributed to CSB of the nuclear force.

We have applied the three different CSB forces presented in the previous section in accurate momentum-space Faddeev calculations of the three-nucleon systems [32]. Our results for the ^3H - ^3He binding energy differences are shown in the upper part of Table II. We conducted two types of calculations. In the first type, we included CSB only in 1S_0 while all other partial waves are treated charge-symmetric. In the second type, CSB was included in all $T = 1$ partial waves (i. e., distinct pp and nn potentials were used in the $T = 1$ states).

The predictions by the CSB models are between 60 and 66 keV. Thus, they are all consistent with the empirical value of 67 ± 9 keV and no discrimination is possible. Moreover, the CSB contribution beyond 1S_0 is small, 2-5 keV (about 6% of the total), which is within the empirical uncertainty. Therefore, it is impossible to draw any conclusions concerning the CSB contributions from 3P_J waves.

The trends in the results are consistent with the phase shift differences shown in Fig. 4: The ρ - ω model generates more binding energy difference from the 1S_0 state (3.3 keV more) and more from 3P_J waves (2.5 keV more) as compared to the M_N -splitting model.

B. Nolen-Schiffer anomaly

It is a well-known experimental fact that the single-particle energies of corresponding states in mirror nuclei are different. If one assumes that the strong part of the nuclear force is charge symmetric, i.e. the strong proton-proton interaction is identical to the interaction between two neutrons, then these differences would originate entirely from the electromagnetic interaction (mainly Coulomb) between the nucleons. For this reason, it is customary to call these single-particle energy differences the Coulomb displacement energies. After accurate experimental data on the charge distribution became available from electron scattering experiments, Hartree-Fock calculations with phenomenological models for the NN interaction like the Skyrme forces were performed which reproduced these measured charge distributions with good accuracy. The Coulomb displacement energies which were evaluated with these Hartree-Fock wave functions, however, underestimated the experimental data by typically seven percent. This has become known as the Nolen-Schiffer (NS) anomaly [20]. Many attempts have been made to explain this discrepancy by the inclusion of electromagnetic corrections, many-body correlations beyond the Hartree-Fock approximation, or by explicit charge-symmetry breaking terms in the NN interaction [3,37–40]. In these investigations it turned out that the CSB of the nuclear force (with the nn interaction more attractive than the pp one) is probably the major reason for the ‘anomaly’.

We will now study the impact of CSB of the NN interaction on the single-particle energies for protons and neutrons in nuclear matter as well as in finite nuclei.

1. Nuclear matter

We calculate the single-particle potential for protons, $U_p(k)$, and neutrons, $U_n(k)$, as a function of the momentum k in symmetric nuclear matter using the self-consistent Brueckner-Hartree-Fock approach [19]. From this we obtain the CSB energy difference

$$\Delta U_{CSB}(k) \equiv U_p(k) - U_n(k). \quad (3.1)$$

Since the momentum dependence of ΔU_{CSB} is weak, we choose $k = k_F$. Our results at nuclear matter density, $k_F = 1.35 \text{ fm}^{-1}$, are shown in the lower part of Table II. The most encouraging aspect of the results is that, here, we encounter a large contribution from states with $L > 0$ (about 50% of the total). Consequently, we also observe a substantial difference between the model predictions, with the ρ - ω model producing about 20% more energy difference than the M_N -splitting model.

Unfortunately, no reliable empirical estimates for ΔU_{CSB} in nuclear matter exist such that we cannot draw any conclusions. Accurate data exist for finite nuclei which we will consider in the next section.

2. Finite nuclei

We choose ^{16}O for our sample nucleus and we wish to calculate Coulomb displacement energies around this nucleus [41]. Calculations of this kind are very involved and, therefore,

we need to discuss first how to conduct such microscopic nuclear structure calculations in a proper way.

One possibility would be to perform self-consistent Brueckner-Hartree-Fock (BHF) calculations and extract the Coulomb displacement energies from the single-particle energies for protons and neutrons. We do not take this approach, for the following reasons: (i) Such self-consistent BHF calculations typically predict the radii for the charge-density distributions too small [42]. This implies that the leading Coulomb contribution to the displacement energy would be overestimated. Also the calculation of the correction terms would be based on single-particle wavefunctions which are localized too much. (ii) BHF calculations are appropriate for short-range correlations. However, long-range correlations involving the admixture of configurations with low excitation energies in the uncorrelated shell-model basis require a more careful treatment. (iii) The BHF single-particle energies do not account for any distribution of the single-particle strength consistent with realistic spectral functions.

For the reasons listed, we take the following approach. We use single-particle wave functions from Hartree-Fock calculations with effective nuclear forces, which yield a good fit to the empirical charge distribution. These wave functions are used to determine the leading Coulomb contribution and corrections like the effects of finite proton size, the electromagnetic spin-orbit interaction, the kinetic energy correction due to the mass difference between proton and neutron, and the effects of vacuum polarization. Actually, for these contributions we use the results by Sato [38]. The first column of our Table III is taken from table 2 of Ref. [38] which includes all the effects just mentioned.

The correlation effects are taken into account in a two-step procedure. We assume a model space defined in terms of shell-model configurations including oscillator single-particle states up to the $1p0f$ shell. We use the oscillator parameter $b = 1.76$ fm which is appropriate for ^{16}O . The effects of short-range correlations are calculated by employing an effective interaction, i.e. a \mathcal{G} -matrix suitable for the model space. This \mathcal{G} -matrix is determined as the solution of the Bethe-Goldstone equation

$$\mathcal{G}(\Omega) = V + V \frac{Q_{\text{mod}}}{\Omega - Q_{\text{mod}} T Q_{\text{mod}}} \mathcal{G}(\Omega), \quad (3.2)$$

where T is identified with the kinetic energy operator, while V stands for the bare two-body interaction including the Coulomb interaction and accounting for CSB in the strong interaction. The Pauli operator Q_{mod} in this Bethe-Goldstone Eq. (3.2) is defined in terms of two-particle harmonic oscillator states $|\alpha\beta\rangle$ by

$$Q_{\text{mod}}|\alpha\beta\rangle = \begin{cases} 0 & \text{if } \alpha \text{ or } \beta \text{ from } 0s \text{ or } 0p \text{ shell} \\ 0 & \text{if } \alpha \text{ and } \beta \text{ from } 1s0d \text{ or } 1p0f \text{ shell} \\ |\alpha\beta\rangle & \text{elsewhere} \end{cases} \quad (3.3)$$

As a first approximation we use the resulting \mathcal{G} -matrix elements and evaluate single-particle energies in the BHF approximation ϵ_α . This approximation, which will be denoted as BHF in the discussion below, accounts for short-range correlations, which are described in terms of configurations outside our model space. In a next step we add to this BHF definition of the nucleon self-energy the irreducible terms of second order in \mathcal{G} which account for intermediate two-particle one-hole and one-particle two-hole configurations within the model-space

$$\mathcal{U}_\alpha^{(2)} = \frac{1}{2} \sum_{p_1, p_2, h} \frac{\langle \alpha h | \mathcal{G} | p_1 p_2 \rangle \langle p_1 p_2 | \mathcal{G} | \alpha h \rangle}{\omega - (\epsilon_{p_1} + \epsilon_{p_2} - \epsilon_h) + i\eta} + \frac{1}{2} \sum_{h_1, h_2, p} \frac{\langle \alpha p | \mathcal{G} | h_1 h_2 \rangle \langle h_1 h_2 | \mathcal{G} | \alpha p \rangle}{\omega - (\epsilon_{h_1} + \epsilon_{h_2} - \epsilon_p) - i\eta}. \quad (3.4)$$

Applying the techniques described in [43], we can solve the Dyson equation for the single-particle Greens function $G_\alpha(\omega)$

$$G_\alpha(\omega) = g^\alpha(\omega) + g_\alpha(\omega) \mathcal{U}_\alpha^{(2)}(\omega) G_\alpha(\omega) \quad (3.5)$$

with g_α the BHF approximation for the single-particle Greens function, and determine its Lehmann representation

$$G_\alpha(\omega) = \sum_n \frac{|\langle \Psi_n^{A+1} | a_\alpha^\dagger | \Psi_0 \rangle|^2}{\omega - (E_n^{A+1} - E_0) + i\eta} + \sum_m \frac{|\langle \Psi_m^{A-1} | a_\alpha | \Psi_0 \rangle|^2}{\omega - (E_0 - E_m^{A-1}) - i\eta}. \quad (3.6)$$

This yields directly the energies of the states with $A \pm 1$ nucleons that we are interested in.

Our results for the Coulomb displacement energies are listed in Table III for various one-hole and one-particle states relative to ^{16}O . The first column of this table, $C^{(1)}$, contains the results of Ref. [38] for the leading Coulomb contributions, the corrections due to the finite proton size, the electromagnetic spin-orbit interaction, the kinetic energy correction due to nucleon mass splitting, and the effects of vacuum polarization. As discussed above, we think that it is more realistic to evaluate these contributions for single-particle wave functions which are derived from Hartree-Fock calculations with phenomenological forces rather than using the wavefunctions derived from a microscopic BHF calculation.

The second and third columns of Table III list the corrections to the Coulomb displacement energies which originate from the treatment of short-range (Δ_{SR}) and long-range correlations (Δ_{LR}) discussed above. The correction Δ_{SR} has been derived from the differences of BHF single-particle energies for protons and neutrons subtracting the Coulomb displacement energy evaluated in the mean-field approximation

$$\Delta_{SR} = \epsilon_i^{BHF}(\text{proton}) - \epsilon_i^{BHF}(\text{neutron}) - \Delta_{\text{mean field}} \quad (3.7)$$

In this case the BHF calculations have been performed with the np versions of the different interactions. The correction terms Δ_{LR} have been evaluated in a similar way from the quasiparticle energies determined in the Greens function approach, subtracting the BHF effects already contained in Δ_{SR} . The correction terms Δ_{SR} and Δ_{LR} include the effects represented by irreducible diagrams of second and higher order in the interaction, in which at least one of the interaction lines represents the Coulomb interaction. In addition they contain the effects of folded diagrams discussed by Tam et al. [40]. We find that the correlation effects are rather weak. The short- and long-range contributions tend to cancel each other. This is true in particular for the one-hole states $p_{3/2}^{-1}$ and $p_{1/2}^{-1}$. The effects of short-range correlations dominate in the case of the particle states, $d_{5/2}$ and $1s_{1/2}$, leading to a total correlation effect in the order of 100 keV in the Coulomb displacement energies. This effect is slightly larger for the Argonne potential than for the Bonn potentials because of the stronger correlations in the case of Argonne.

The contributions to the Coulomb displacement energies caused by CSB of the NN interactions, Δ_{CSB} , are listed in the fourth column of Table III. We have conducted separate calculations for each of the three models for CSB introduced in Sec. II.

We note that, also in the calculations of the Coulomb displacement energies, it is important to include CSB beyond the 1S_0 state in the NN interaction. Similarly to what we found for the nuclear matter ΔU_{CSB} (cf. Sec. III.B.1 and lower part of Table II), CSB in P and higher partial waves contributes about 50% of the total Δ_{CSB} . This was demonstrated in Ref. [41].

We achieve satisfactory or even good agreement in some cases, like $p_{3/2}^{-1}$ and $1s_{1/2}$, but there are discrepancies in others. For $p_{1/2}^{-1}$ and $d_{5/2}$ the remaining discrepancies are larger than the Δ_{CSB} contribution.

The general trend in the results is that the ρ - ω model generates about 10-20% more Δ_{CSB} than the M_N -splitting mechanism, and Argonne V_{18} is, in general, in-between the two. Even though the ρ - ω trend is a favourable one, it is not sufficiently pronounced such that one could give a preference to this model. In the critical cases, like $p_{1/2}^{-1}$ and $d_{5/2}$, the discrepancies between all model predictions, on the one hand, and experiment, on the other, are much larger than the differences within the model predictions.

Concerning the remaining discrepancy, a comment is in place. Note that the nuclear structure part of our calculations may carry some uncertainty. This is true in particular for the evaluation of the leading Coulomb contribution, which is sensitive to the Hartree-Fock wave functions which are used. To obtain an idea of how large such uncertainties may be, we compare the results for Coulomb displacement energies using the Skyrme II force and *no CSB* by Sato [38] with the more recent ones by Suzuki *et al.* [44]. For the single-hole state $p_{1/2}^{-1}$, Suzuki's result is larger by 167 keV as compared to Sato; and for the single-particle state $d_{5/2}$, the two calculations differ by 138 keV. Uncertainties of this size can well explain the remaining discrepancies in our results.

IV. SUMMARY AND CONCLUSIONS

We have tested three different models for the charge symmetry breaking (CSB) of the NN interaction. The models are based upon ρ - ω mixing, nucleon mass (M_N) splitting, and phenomenology (Argonne V_{18}). All models reproduce the empirical value for the CSB of the 1S_0 scattering length (Δa_{CSB}) accurately.

We reveal that there are considerable differences in the predictions by these models for CSB in 3P_J waves. We have investigated the impact of these differences on some observable quantities of $A \geq 3$ nuclear systems that are sensitive to CSB of the nuclear force.

We find that the ^3H - ^3He binding energy difference is essentially ruled by Δa_{CSB} and that P and higher partial waves contribute only about 6%. Therefore, this quantity is unsuitable to discriminate between different models for CSB of the nuclear force.

A test calculation conducted for nuclear matter shows that in heavier nuclear systems the difference between proton and neutron single-particle energies receives about 50% from partial waves other than 1S_0 . Motivated by this result, we have calculated the Coulomb displacement energies around the closed shell nucleus ^{16}O . We find that the contribution to these energy differences from CSB of the NN interaction (which is in the order of 100 keV) differs by 10-20% among the three models for CSB, which is appreciable. Unfortunately,

the nuclear structure part of these calculations, in particular the evaluation of the leading Coulomb contributions, carry an uncertainty in the order of 100 keV such that the subtle differences between the competing CSB models get swamped. Therefore we must conclude that, based upon the calculations conducted in this study, we are unable to give preference to any of the three CSB models.

What we need are observables for which the nuclear structure part is fully under control. This suggests to look into nuclear few-body reactions for which exact calculations can be performed [45]. An example could be the analyzing power, A_y , in nucleon-deuteron scattering that is known to depend sensitively on the 3P_J waves of the NN potential. Accurate data on $p-d$ and $n-d$ A_y exist and these data exhibit a clear signature of CSB. Unfortunately, these data cannot be explained without recourse to three-body forces which may obscure the CSB aspect of the problem. In any case, we like to encourage the nuclear few-body community [45] to identify spin observables in few-body reactions that show sensitivity to CSB of the NN interaction, particularly, the one that comes from 3P_J waves. Investigations of this kind may ultimately allow to discriminate between competing models for CSB of the nuclear force.

ACKNOWLEDGMENTS

This work was supported in part by the U.S. National Science Foundation under Grant No. PHY-9603097 and by the German DFG (SFB 382).

REFERENCES

- [1] C. R. Howell *et al.*, Phys. Lett. **B444**, 252 (1998).
- [2] D. E. González Trotter *et al.*, Phys. Rev. Lett. **83**, 3788 (1999).
- [3] G. A. Miller, M. K. Nefkens, and I. Slaus, Phys. Rep. **194**, 1 (1990).
- [4] R. Machleidt, Adv. Nucl. Phys. **19**, 189 (1989).
- [5] G. A. Miller and W. H. T. van Oers, In *Symmetries and Fundamental Interactions in Nuclei*, W. C. Haxton and E. M. Henley, eds. (World Scientific, Singapore, 1995) p. 127.
- [6] S. A. Coon and R. C. Barrett, Phys. Rev. C **36**, 2189 (1987).
- [7] S. A. Coon and M. D. Scadron, Phys. Rev. C **26**, 562 (1982).
- [8] T. Goldman, J. A. Henderson, and A. W. Thomas, Few-Body Systems **12**, 193 (1992).
- [9] J. Piekarewicz and A. G. Williams, Phys. Rev. C **47**, 2462 (1993).
- [10] G. Krein, A. W. Thomas, and A. G. Williams, Phys. Lett. **B317**, 293 (1993).
- [11] H. B. O’Connell, B. C. Pearce, A. W. Thomas, A. G. Williams, Phys. Lett. **B336**, 1 (1994).
- [12] S. A. Coon, B. H. J. McKellar, and A. A. Rawlinson, Proc. 6th Conf. Intersections between Nuclear and Particle Physics, AIP Conf. Proc. **412**, ed. T. W. Donnelly (AIP, Woodbury, 1997) p. 368.
- [13] H. B. O’Connell, B. C. Pearce, A. W. Thomas, A. G. Williams, Prog. Part. Nucl. Phys. **39**, 201 (1997).
- [14] S. A. Coon and M. D. Scadron, *Charge symmetry breaking via $\Delta I = 1$ group theory or by the u - d quark mass difference and direct photon exchange*, Proc. XXIII Symposium on Nuclear Physics, Oaxtepec, Mexico, January 2000, Revista Mexicana de Fisica, to be published.
- [15] R. Machleidt, K. Holinde, and Ch. Elster, Phys. Rep. **149**, 1 (1987).
- [16] S. A. Coon and J. A. Niskanen, Phys. Rev. C **53**, 1154 (1996).
- [17] G. Q. Li and R. Machleidt, Phys. Rev. C **58**, 1393 (1998).
- [18] U. van Kolck, M. C. M. Rentmeester, J. L. Friar, T. Goldman, and J. J. de Swart, Phys. Rev. Lett. **80**, 4386 (1998).
- [19] H. Müther, A. Polls, and R. Machleidt, Phys. Lett. **B445**, 259 (1999).
- [20] J. A. Nolen and J. P. Schiffer, Annu. Rev. Nucl. Sci. **19**, 471 (1969).
- [21] R. B. Wiringa, V. G. J. Stoks, and R. Schiavilla, Phys. Rev. C **51**, 38 (1995).
- [22] P. C. McNamee, M. D. Scadron, and S. A. Coon, Nucl. Phys. **A249**, 483 (1975).
- [23] R. Blankenbecler and R. Sugar, Phys. Rev. **142**, 1051 (1966).
- [24] E. E. Salpeter and H. A. Bethe, Phys. Rev. **84**, 1232 (1951).
- [25] R. Machleidt, *The high-precision, charge-dependent, Bonn nucleon-nucleon potential (CD-Bonn)*, arXiv:nucl-th/0006014; this is an update of: R. Machleidt, F. Sammarruca, and Y. Song, Phys. Rev. C **53**, R1483 (1996).
- [26] Review of Particle Physics, Eur. Phys. J. C **3**, 1 (1998).
- [27] The convention used in Ref. [6] for g_α^2 differs by a factor of four from ours.
- [28] R. V. Reid, Ann. Phys. (N.Y.) **50**, 411 (1968).
- [29] Based upon the Bonn Full Model [15], the original investigation [17] of the effect of nucleon mass splitting uses the πNN coupling constant $g_\pi^2/4\pi = 14.4$ which is not current. For that reason we have revised the Bonn Full Model using $g_\pi^2/4\pi = 13.6$ and then repeated the CSB calculations of Ref. [17]. The total Δa_{CSB} predicted by the revised model is 1.508 fm (about 5% less than what was reported in Ref. [17]).

- Similarly, the phase shift differences created by nucleon mass splitting shown in Fig. 4 by the dashed curve are, in general, a few percent smaller than those given in Ref. [17].
- [30] W. A. van der Sanden, A. H. Emmen, and J. J. de Swart, Report No. THEF-NYM-83.11, Nijmegen, 1983, unpublished; quoted in Ref. [31].
 - [31] J. R. Bergervoet, P. C. van Campen, W. A. van der Sanden, and J. J. de Swart, Phys. Rev. C **38**, 15 (1988).
 - [32] R. A. Brandenburg, G. S. Chulick, Y. E. Kim, D. J. Klepacki, R. Machleidt, A. Picklesimer, and R. M. Thaler, Phys. Rev. C, **37**, 781 (1988).
 - [33] J. L. Friar, B. F. Gibson, and G. L. Payne, Phys. Rev. C **35**, 1502 (1987).
 - [34] Y. Wu, S. Ishikawa, and T. Sasakawa, Phys. Rev. Lett. **64**, 1875 (1990).
 - [35] R. A. Brandenburg, S. A. Coon, and P. U. Sauer, Nucl. Phys. **A294**, 305 (1978).
 - [36] J. L. Friar, B. F. Gibson, and G. L. Payne, Phys. Rev. C **42**, 1211 (1990).
 - [37] N. Auerbach, J. Hüfner, C.M. Shakin, and A.K. Kerman, Rev. Mod. Phys. **44**, 48 (1972).
 - [38] H. Sato, Nucl. Phys. **A 269**, 378 (1976).
 - [39] P.G. Blunden and M.J. Iqbal, Phys. Lett. **B 198**, 14 (1987).
 - [40] K.C. Tam, H. Müther, H.M. Sommermann, T.T.S. Kuo, and A. Faessler, Nucl. Phys. **A 361**, 412 (1981).
 - [41] C. Harzer, H. Müther, and R. Machleidt, Phys. Lett. **B459**, 1 (1999).
 - [42] K.W. Schmid, H. Müther, and R. Machleidt, Nucl. Phys. **A530**, 14 (1991).
 - [43] H. Müther and L.D. Skouras, Nucl. Phys. **A581**, 247 (1995).
 - [44] T. Suzuki, H. Sagawa, and A. Arima, Nucl. Phys. **A536**, 141 (1992).
 - [45] W. Glöckle, H. Witala, D. Hüber, H. Kamada, J. Golak, Phys. Rep. **274**, 107 (1996), and references therein.

TABLES

TABLE I. 1S_0 scattering length (a) and effective range (r), for proton-proton (pp) and neutron-neutron (nn), with Coulomb effects (C) and without any electromagnetic effects (N), in units of fm.

	ρ - ω mixing	M_N splitting	Argonne V_{18}	Experiment
a_{pp}^C	-7.8154	-7.8154	-7.8138	-7.8149 ± 0.0029^a
r_{pp}^C	2.773	2.773	2.787	2.769 ± 0.014^a
a_{pp}^N	-17.460	-17.460	-17.164	
r_{pp}^N	2.845	2.845	2.865	
a_{nn}^N	-18.968	-18.968	-18.818	-18.9 ± 0.4^b
r_{nn}^N	2.816	2.819	2.834	2.75 ± 0.11^c
Δa_{CSB}	1.508	1.508	1.654	1.6 ± 0.6
Δr_{CSB}	0.029	0.026	0.031	0.10 ± 0.12

^aReference [30].

^bReference [1,2].

^cReference [3].

TABLE II. Applications of CSB potentials in the three-nucleon system and in symmetric nuclear matter.

	ρ - ω mixing	M_N splitting	Argonne V_{18}	Empirical
^3H-^3He binding energy difference (keV)				
CSB in 1S_0 only	60.9	57.6	62.1	
CSB in all $T = 1$ states	65.8	60.0	65.1	67 ± 9
Nuclear matter ΔU_{CSB} (MeV)				
CSB in 1S_0 only	0.168	0.154	0.180	
CSB in all $T = 1$ states	0.367	0.311	0.301	

TABLE III. Coulomb displacement energies for single-hole ($p_{3/2}^{-1}$ and $p_{1/2}^{-1}$) and single-particle states ($d_{5/2}$ and $1s_{1/2}$) around ^{16}O . The single-particle contribution, $C^{(1)}$, is from Sato [38]. Contributions due to short-range correlations, Δ_{SR} , long-range correlations inside the model space, Δ_{LR} , and due to CSB of the strong interaction, Δ_{CSB} , are calculated for three different CSB models. The total results for the displacement energies, C^{Tot} , are compared to the experimental data given in the last column. All entries are in keV.

		$C^{(1)}$	Δ_{SR}	Δ_{LR}	Δ_{CSB}	C^{Tot}	Exp
$p_{3/2}^{-1}$	ρ - ω mixing	3205	-44	46	106	3313	3395
	M_N splitting		-44	46	97	3303	
	Argonne V_{18}		-71	47	108	3285	
$p_{1/2}^{-1}$	ρ - ω mixing	3235	-52	37	124	3344	3542
	M_N splitting		-52	37	102	3322	
	Argonne V_{18}		-79	39	103	3297	
$d_{5/2}$	ρ - ω mixing	3135	154	-15	93	3367	3542
	M_N splitting		154	-15	87	3361	
	Argonne V_{18}		187	-18	92	3401	
$1s_{1/2}$	ρ - ω mixing	2905	159	-45	134	3154	3166
	M_N splitting		160	-46	112	3132	
	Argonne V_{18}		198	-47	112	3174	

FIGURES

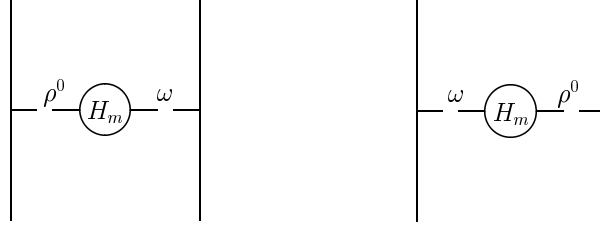


FIG. 1. ρ^0 - ω exchange contributions to the nuclear force that violate charge symmetry.

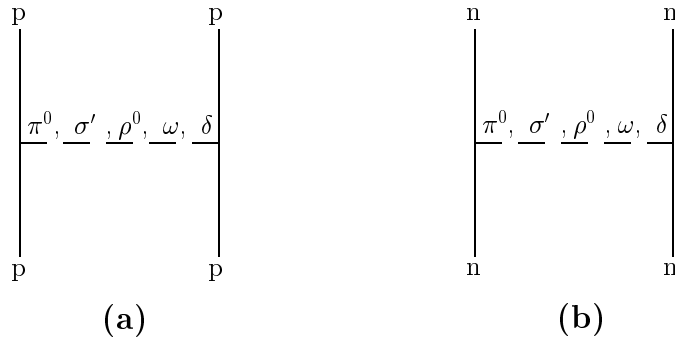
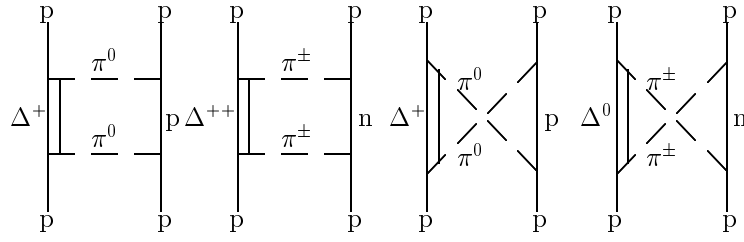
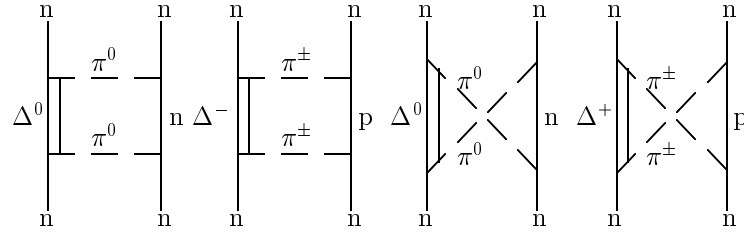


FIG. 2. One-boson-exchange (OBE) contributions to (a) pp and (b) nn scattering.



(a)



(b)

FIG. 3. Two-pion-exchange contributions with $N\Delta$ intermediate states to (a) pp and (b) nn scattering.

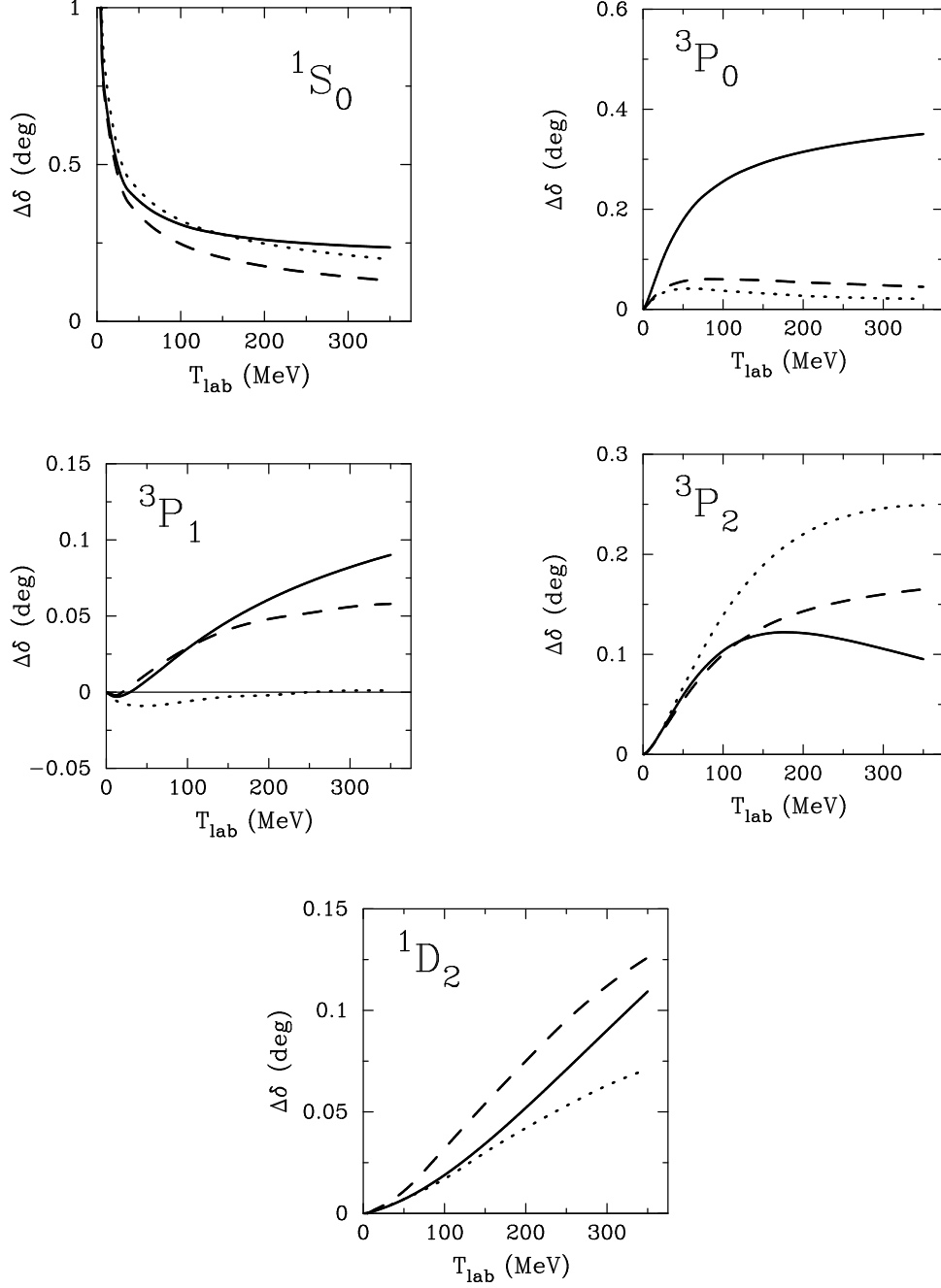


FIG. 4. CSB phase shift differences $\delta_{nn} - \delta_{pp}$ (without electromagnetic interactions) for laboratory kinetic energies T_{lab} below 350 MeV and partial waves with $L \leq 2$ as generated by ρ - ω mixing (solid line), nucleon mass splitting (dashed), and the phenomenological Argonne V_{18} model (dotted).